RESEARCH PAPERS

Acta Cryst. (1995). A**51**, 651–658

An Accurate Determination of the Thermal Vibration of Rutile from the Nuclear Density Distribution of the Maximum-Entropy Analysis

BY SHINTARO KUMAZAWA

Department of Physics, Science University of Tokyo, Noda, Chiba 278, *Japan*

AND MASAKI TAKATA AND MAKOTO SAKATA

Department of Applied Physics, Nagoya University, Nagoya 464-01, *Japan*

(*Received* 12 *October* 1994; *accepted* 25 *January* 1995)

Abstract

The maximum-entropy method (MEM) can provide a high-resolution nuclear density distribution purely from experimental neutron diffraction data. The distribution expresses thermal smearing, which is caused by all kinds of thermal-vibration modes both harmonic and anharmonic. If the effective one-particle potential (OPP) is assumed to describe thermal smearing of nuclei, the potential parameters can be determined by least-squares refinement of the nuclear density distribution. By this method, the OPP parameters of rutile (TiO_2) are directly determined from the nuclear density distribution originally derived by Sakata, Uno, Takata & Howard [*J. Appl. Cryst.* (1993), **26**, 159–164]. In the rutile case, the x coordinate of the O atom located at $(x, x, 0)$ has to be determined before the OPP parameters are analysed. The atomic position is defined as the position where the first-order moment of the nuclear density becomes zero. The obtained x coordinate is 0.30477, which shows excellent agreement with the previous study of Rietveld analysis by Howard, Sabine & Dickson [*Acta Cryst.* (1991), B**47**, 462–468], *i.e.* 0.30478 (6). The higher-order moments of nuclear density are calculated in order to build an adequate OPP model. Among these values, none of the sixth order is significant and hence the OPP model up to fourth-order anharmonicity is employed. The potential parameters are refined by least-squares analysis using the above OPP model. For the Ti atom, nine OPP parameters (three harmonic and six fourth-order anharmonic) are determined with reliability factor $R = 0.73\%$. For the O atom, twelve OPP parameters (three harmonic, three third- and six fourth-order anharmonic) are determined with $R = 3.83\%$. The nuclear density of the O atom shows substantial skewness in rutile owing to the third-order anharmonicities. It is shown that the present method is a very powerful technique to determine the precise values for both harmonic and anharmonic potential parameters based on the OPP model in comparison with conventional structure analysis.

1. Introduction

Sakata & Sato (1990) have proposed a new accurate structure analysis technique, that is, the maximum-entropy method (MEM). It is demonstrated that the MEM analysis of X-ray diffraction data is a very powerful method to visualize the detail of electron-density distribution without using a structural model. The number of examples in which the MEM has been successfully applied to obtain accurate electron-density distributions are rapidly increasing, *e.g.* Si (Sakata & Sato, 1990), CeO_2 (Sakata, Mori, Kumazawa, Takata & Toraya, 1990), TiO_2 (Sakata, Uno, Takata & Mori, 1992) and Mg (Kubota, Takata & Sakata, 1993) *etc.* When the MEM is applied to neutron diffraction data for a non-magnetic elastic scattering measurement, it can yield a high-resolution nuclear density distribution in the same way, *e.g.* Be (Takata, Sakata, Kumazawa, Larsen & Iversen, 1994), TiO_2 (rutile) (Sakata, Uno, Takata & Howard, 1993), TiO_2 (anatase) (Sakata, Uno, Takata, Takagi, Kumazawa & Howard, 1994) *etc.* In the neutron diffraction case, the distribution is equivalent to the atomic thermal smearing function (TSF), which is caused by all kinds of thermal-vibration modes of constituent atoms because the spatial breadth of nuclei can be neglected. One of the most convenient methods for describing the TSF is to assume that the atom is vibrated by a self-consistent molecular field, which is called the effective one-particle potential (OPP). By using the OPP model, it is, in principle, possible to determine the harmonic and anharmonic potential parameters by least-squares refinement of the nuclear-density distribution obtained by the MEM. This will give us an alternative method of determining thermal parameters.

In conventional structure analysis, the anharmonic thermal parameters are included in temperature factors. According to Willis (1969), the TSF is defined as the Boltzman distribution of vibrational potential by using the OPP model and the temperature factor is a Fourier transformation of the TSF. This Fourier transformation

cannot be solved analytically and thus the approximation in which the TSF is expanded by the Taylor series had to be introduced. In the approximation, the anharmonic terms are regarded as a small perturbation, which may not be the case in a real crystal. In the present analysis, it is not necessary to calculate the temperature factor, since the analysis of potential parameters is carried out in real space. Therefore, the analysis is free from the limitation that comes from the approximation introduced to perform the Fourier transformation of TSF.

In this work, the OPP parameters of rutile (TiO_2) are directly determined from the MEM nuclear density distribution. This work is only the second example of such an analysis. The first example is the single-crystal neutron diffraction data of Be by Takata, Sakata, Kumazawa, Larsen & Iversen (1994). Although the principal idea of the potential parameter analysis is the same as in the Be case, the present work deals with a more general case. For example, the atomic position has to be evaluated from the nuclear-density distribution before analysing the potential parameters. In the Be case, the atomic position is fixed at a special position by symmetry requirements. Therefore, the detailed theoretical background of analysis will be repeated in this paper. The MEM nuclear density distribution to be analysed in this work is obtained from the powder diffraction data. It is very unusual to carry out an analysis of anharmonic potential parameters with powder data. In the conventional method, severe correlations between potential parameters would prevent such an analysis being performed. This work shows that it is possible to obtain anharmonic potential parameters from powder data by the present method.

2. Rutile structure and the MEM density maps

The unit cell of rutile (TiO_2) is shown in Fig. 1. The structure is tetragonal and the space group is $P4_2/mnm$ (No. 136) with lattice constants $a = 4.594$ and $c = 2.959$ Å at room temperature (Howard, Sabine & Dickson, 1991). In this structure, the Ti atom is located at position (0, 0, 0), which is the special position with *mmm* point-group symmetry and the O atom is located at position $(x, x, 0)$ with *mm*2 point-group symmetry. In order to determine the potential parameters, the displacements of each atom are represented by the principal-axes system, u_x, u_y and u_z, of which the origin is the atomic position. The precision of the present analysis strongly depends on the accuracy of this origin. Therefore, it is important to know the precise atomic position of the O atom. In §3, the procedure to determine the atomic position from the MEM nuclear density distribution will be mentioned in detail.

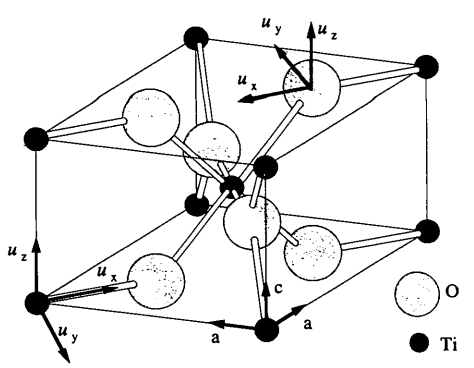

Fig. 1. The rutile structure and the principal axes representing atomic displacements for the Ti and O atoms.

The nuclear density distributions of rutile at room temperature was originally obtained with $64 \times 64 \times 64$ pixels by Sakata, Uno, Takata & Howard (1993). The neutron powder diffraction data used in the MEM analysis has been analysed by the Rietveld method (Howard, Sabine & Dickson, 1991). The nuclear density is usually distributed within a limited space around the atomic position. There are a small number of pixels in such a tiny region. In order to analyse the higher-order anharmonic terms precisely, finer pixels are needed. Therefore, the MEM analysis was carried out again with $128 \times 128 \times 128$ pixels using the new computer program *MEND*, which has been developed for analysing neutron diffraction data with negative scattering length, such as for the Ti atom, and employs a new efficient algorithm, which is initially applied to the computer program *MEED* (Kumazawa, Kubota, Takata, Sakata & Ishibashi, 1993). This can analyse the X-ray diffraction data and the neutron diffraction data with positive scattering lengths only. By using *MEND*, a large computation, such as the $128 \times 128 \times 128$ pixels case, can be performed without any difficulties. In the present calculation, the supercomputer FACOM VP2600 at Nagoya University Computation Center was used. The total computing CPU time was 11 s for 32 iteration cycles. The obtained MEM nuclear-density maps are shown in Figs. 2(*a*) and (*b*), which are (110) and (002) planes, respectively. These maps are essentially the same as the previous MEM calculation except for the resolution of the pixels.

3. Theory

As mentioned in §1, the procedure for potential analysis has to be extended. In order to clarify each procedure, a flow chart is shown in Fig. 3. Of the four procedures, steps 1, 2 and 4 are the newly added parts not included in the previous study of Be.

Step 1 is to calculate the atomic position from the MEM nuclear density distribution. In the rutile case, the corresponding atom is the O atom that is located at $(x, x, 0)$. In order to determine the atomic position purely from the nuclear densities, the atomic position has to be defined from the nuclear density distribution. In this work, the atomic position, $\mathbf{r}_c$, is defined as the position for which the first-order moment of nuclear density

becomes zero. The first-order moment is given as

$$L(\mathbf{r}_c) = \int \mathbf{u}\rho_{\mathrm{MEM}}(\mathbf{r}_c + Q^{-1}\mathbf{u})\,du_x\,du_y\,du_z, \quad (1)$$

where $\mathbf{u}$ is an atomic displacement defined in the principal-axis system, Q is a transformation matrix that converts from the crystal axes to the principal axes and ρ_{MEM} is the MEM nuclear density distribution. In the calculation, the integration in (1) is substituted into the summation over the finite sphere region with radius R_0 since ρ_{MEM} is derived as a discrete form.

$$L(\mathbf{r}_c) = \sum_{u^2 \le R_0^2} \mathbf{u}\rho_{\mathrm{MEM}}(\mathbf{r}_c + Q^{-1}\mathbf{u}). \quad (2)$$

Equation (2) is the step function with 1 pixel resolution. It is found that even 128 × 128 × 128 pixels is not fine enough to determine the atomic position with good accuracy. Therefore, ρ_{MEM} is interpolated by the following equation (Sakurai, 1972).

$$\begin{aligned}\rho_{\mathrm{MEM}}(\mathbf{r}) &= \rho_{\mathrm{MEM}}(x_m + p, y_m + q, z_m + r)\\ &= (1-q)\{(1-r)[(1-p)\rho_{\mathrm{MEM}}(x_m, y_m, z_m)\\ &\quad + p\rho_{\mathrm{MEM}}(x_{m+1}, y_m, z_m)]\\ &\quad + r[(1-p)\rho_{\mathrm{MEM}}(x_m, y_m, z_{m+1})\\ &\quad + p\rho_{\mathrm{MEM}}(x_{m+1}, y_m, z_{m+1})]\}\\ &\quad + q\{(1-r)[(1-p)\rho_{\mathrm{MEM}}(x_m, y_{m+1}, z_m)\\ &\quad + p\rho_{\mathrm{MEM}}(x_{m+1}, y_{m+1}, z_m)]\\ &\quad + r[(1-p)\rho_{\mathrm{MEM}}(x_m, y_{m+1}, z_{m+1})\\ &\quad + p\rho_{\mathrm{MEM}}(x_{m+1}, y_{m+1}, z_{m+1})]\}, \end{aligned} \quad (3)$$

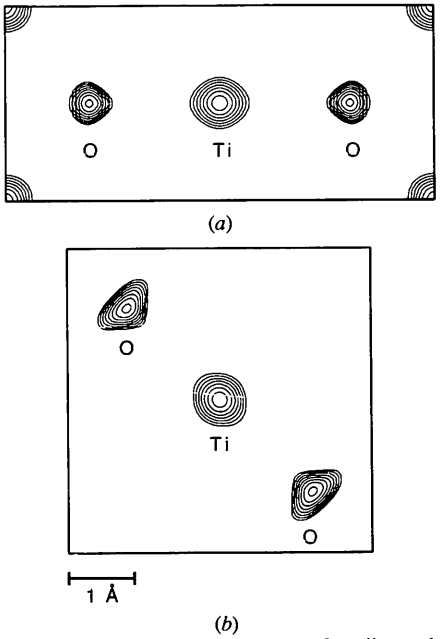

Fig. 2. The MEM nuclear density maps of rutile analysed with 128 × 128 × 128 pixels. (*a*) and (*b*) are (110) and (002) planes, respectively. The contour lines are on a logarithmic scale at 0.01×5^n ($n = 0, 1, ..., 8$) (N Å^{-3}).

where x_m, y_m and z_m are integer values that show the mth pixel's values and p, q and r are half-integer values that show the interpixel positions.

Step 2 is to build the OPP model function by estimating the effective potential order. For this purpose, the higher-order moments are calculated from the MEM nuclear-density distribution. The higher-order moments are given as

$$\langle \mathbf{u}^n \rangle_{\mathrm{MEM}} = \sum_{u^2 \le R_0^2} \mathbf{u}^n \rho'_{\mathrm{MEM}}(\mathbf{u}) \Big/ \sum_{u^2 \le R_0^2} \rho'_{\mathrm{MEM}}(\mathbf{u}), \quad (4)$$

where $\rho'_{\mathrm{MEM}}(\mathbf{u})$ is defined as $\rho_{\mathrm{MEM}}(\mathbf{r}_c + Q^{-1}\mathbf{u})$ with $\mathbf{r}_c$ fixed at the atomic position that is determined in step 1. Equation (4) is also approximated by the summation as in (2) and ρ_{MEM} is also interpolated by (3). The higher-order moments are strongly related to the anharmonicities and thus the significant terms among the obtained

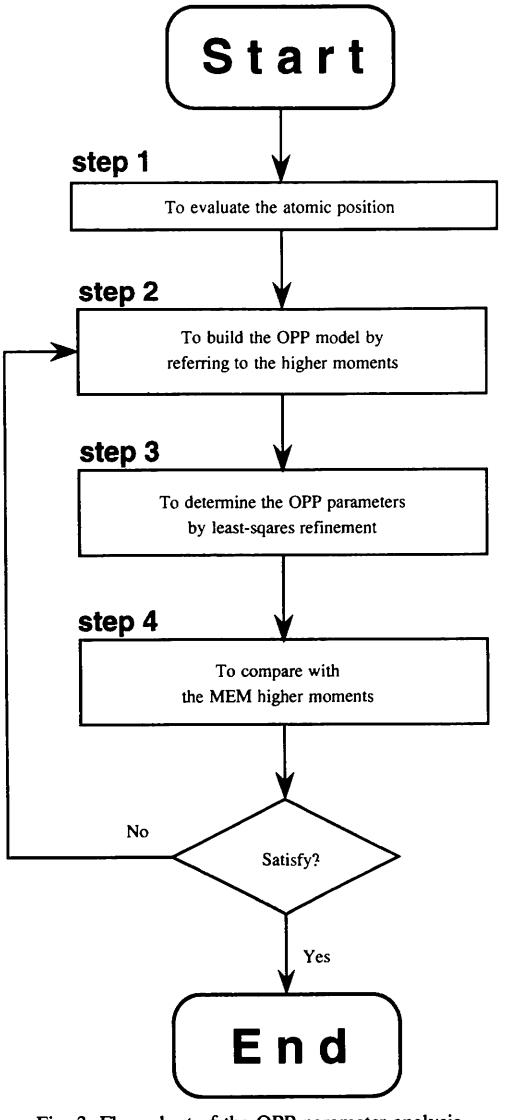

Fig. 3. Flow chart of the OPP parameter analysis.

higher-order moments are employed for the potential analysis.

Step 3 is to determine the potential parameters by least-squares refinement of the MEM nuclear density distribution. The TSF is assumed to be the Boltzman distribution function by using the OPP model with the classical high-temperature approximation and given as

$$\rho_{\mathrm{OPP}}(\mathbf{u}) = A \exp(-V_{\mathrm{OPP}}(\mathbf{u})/k_B T), \qquad (5)$$

where k_B is the Boltzman constant, T the absolute temperature, V_{OPP} the effective one-particle potential, which is defined up to the effective potential order estimated in step 2. A is the normalized factor and is given as the analytical form

$$A = b/\int \exp(-V_{\mathrm{OPP}}(\mathbf{u})/k_B T)\, du_x\, du_y\, du_z, \qquad (6)$$

where b is the scattering length of the corresponding atom. On the other hand, A is the peak maximum of the nuclear density at $\mathbf{u} = 0$. In the present study, A is treated as a least-squares parameter since it may not always agree with the peak maximum of the nuclear density because of discreteness of the MEM nuclear-density distribution. The convergence of the least-squares refinement is evaluated by the following equations:

$$W = \sum_{u^2 \le R_0^2} \omega(\mathbf{u})[\rho'_{\mathrm{MEM}}(\mathbf{u}) - \rho_{\mathrm{OPP}}(\mathbf{u})]^2, \qquad (7)$$

where

$$\omega(\mathbf{u}) = 1/\rho'_{\mathrm{MEM}}(\mathbf{u}). \qquad (8)$$

Equation (8) is the weighting factor of (7). This term is introduced to give an overall fitting from peak maximum to background level. Without this term, a good fit is obtained only for peak-maximum regions. A schematic diagram of step 3 is shown in Fig. 4.

Finally, step 4 is to compare the OPP higher-order moments with the MEM ones. The OPP higher-order moments are calculated from the TSF obtained by the least-squares refinement in step 3 and given as

$$\langle \mathbf{u}^n \rangle_{\mathrm{OPP}} = \sum_{u^2 \le R_0^2} \mathbf{u}^n \rho_{\mathrm{OPP}}(\mathbf{u}) \Big/ \sum_{u^2 \le R_0^2} \rho_{\mathrm{OPP}}(\mathbf{u}). \qquad (9)$$

Higher-order moments of the MEM were calculated in step 2. If a satisfactory agreement between the higher-order moments calculated from the MEM and those from the OPP is not obtained, the procedure may be repeated by adding higher-order anharmonic terms that satisfy the point-group symmetry of the corresponding atom. Otherwise, the present analysis of anharmonic thermal vibrations will be ended.

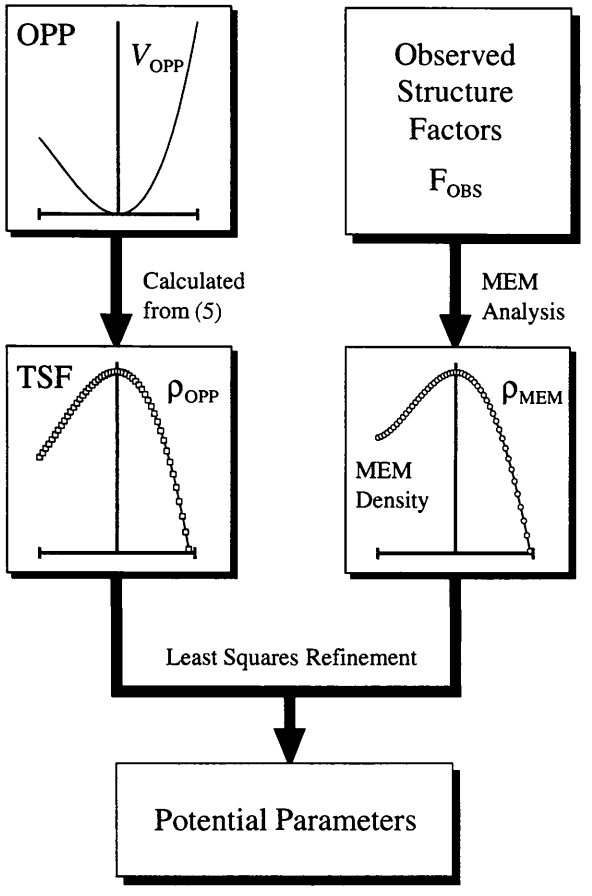

Fig. 4. Schematic diagram of the least-squares refinement.

4. The OPP analysis of rutile

In the rutile case, individual nuclear density distributions of Ti and O atoms are obtained separately because the MEM equation deals with the nuclear density distribution of atoms with positive and negative scattering amplitudes independently (Sakata, Uno, Takata & Howard, 1993). This gives an additional advantage in the present analysis, since the influence of tail densities of a neighbouring atom can be avoided completely. In the case of having only positive or negative scattering amplitudes, a completely separate distribution cannot be obtained. It is considered that the influence of neighbouring atoms is sufficiently small unless the boundary with neighbouring atoms is obscure owing to ionic conductivity or some other reason.

The atomic sites of Ti and O atoms in rutile have point-group symmetry *mmm* and *mm*2, respectively. The principal axes u_x, u_y and u_z are taken to be parallel to the $\langle 110 \rangle$, $\langle 1\bar{1}0 \rangle$ and $\langle 001 \rangle$ crystal axes. Then, the transformation matrix, Q, which converts from the crystal axes to the principal axes, becomes

$$Q = \begin{pmatrix} a\cos\pi/4 & -a\sin\pi/4 & 0 \\ a\sin\pi/4 & a\cos\pi/4 & 0 \\ 0 & 0 & c \end{pmatrix}. \qquad (10)$$

The principal axes of each atom are also indicated in Fig. 1. For the first- and higher-order-moments calculations with (2), (4) and (9), the summation is performed within a sphere of radius 0.6 Å. The difference between the calculated moments within 0.5 and 0.6 Å spheres is negligible. The sphere of radius $R_0 = 0.6$ Å is shown as a dotted circle in Fig. 5(*a*).

In step 1, the atomic position of the O atom is determined from (2). Since the O atom is located at $\mathbf{r}_c = (x_c, x_c, 0)$ in crystal coordinates, $L(\mathbf{r}_c)$ is calculated along the ⟨110⟩ axis as shown in Fig. 5(*a*). The values of $L(\mathbf{r}_c)$ plotted against x_c are shown in Fig. 5(*b*). The solid and dotted lines correspond to the calculated values with and without interpolation [(3)], respectively. Fig. 5(*b*) explains the necessity for the interpolation in the calculation of moments. The determined x_c is 0.30477, which shows excellent agreement with the previous result of Rietveld analysis based on the harmonic model, 0.30478 (6) (Howard, Sabine & Dickson, 1991). This suggests that no significant correlation between the atomic coordinate of the O atom and the potential parameters occurs in the rutile case.

In step 2, the OPP model function is built by using the higher-order moments calculated with (4). For both Ti and O atoms, all values up to sixth order are given in Table 1. None of the sixth-order values is significant. In the present work, the OPP model including up to fourth-order anharmonicities is employed. Hence, the OPP model functions are written for the Ti atom as

$$V_{\mathrm{OPP}} = \alpha_{11}u_x^2 + \alpha_{22}u_y^2 + \alpha_{33}u_z^2 + \gamma_{1111}u_x^4 + \gamma_{2222}u_y^4 + \gamma_{3333}u_z^4 + \gamma_{1122}u_x^2u_y^2 + \gamma_{2233}u_y^2u_z^2 + \gamma_{3311}u_z^2u_x^2 \quad (11)$$

and for the O atom as

$$V_{\mathrm{OPP}} = \alpha_{11}u_x^2 + \alpha_{22}u_y^2 + \alpha_{33}u_z^2 + \beta_{111}u_x^3 + \beta_{221}u_y^2u_x + \beta_{331}u_z^2u_x + \gamma_{1111}u_x^4 + \gamma_{2222}u_y^4 + \gamma_{3333}u_z^4 + \gamma_{1122}u_x^2u_y^2 + \gamma_{2233}u_y^2u_z^2 + \gamma_{3311}u_z^2u_x^2, \quad (12)$$

where α_i, β_i and γ_i are the second-, third- and fourth-order potential parameters. These potentials include all possible terms up to fourth order which satisfy the point-group symmetry of the corresponding atoms (Tanaka & Marumo, 1983).

In step 3, the least-squares refinement of the MEM nuclear density distribution is performed with the above OPP model. In this analysis, the reliability factors of the

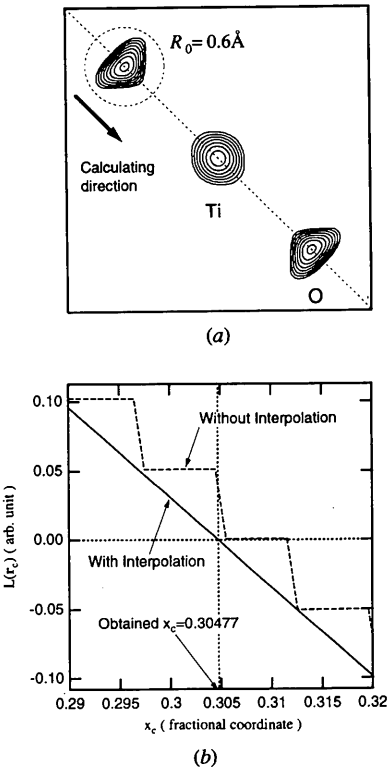

Fig. 5. (*a*) Scheme of calculating the first-order moment for the O atom. (*b*) The first-order moment plotted against x_c. The solid and dotted lines correspond to the calculated values with and without the interpolation [(3)], respectively.

Table 1. *The MEM higher-order moments up to sixth order calculated by the nuclear-density distribution of rutile in the MEM columns and the OPP higher-order moments calculated by the TSF of the fourth-order analysis in the OPP columns*

Units are Å^n × 10^{-3}.

	Ti atom		O atom	
Moments	MEM	OPP	MEM	OPP
$\langle u_x^2\rangle$	6.81	6.80	3.57	3.55
$\langle u_y^2\rangle$	6.20	6.21	7.58	7.56
$\langle u_z^2\rangle$	6.11	6.11	3.82	3.82
$\langle u_x^3\rangle$			−0.016	−0.018
$\langle u_y^2u_x\rangle$			0.095	0.092
$\langle u_z^2u_x\rangle$			0.014	0.014
$\langle u_x^4\rangle$	0.151	0.151	0.040	0.040
$\langle u_y^4\rangle$	0.122	0.122	0.189	0.185
$\langle u_z^4\rangle$	0.118	0.117	0.045	0.045
$\langle u_x^2u_y^2\rangle$	0.044	0.044	0.028	0.028
$\langle u_y^2u_z^2\rangle$	0.041	0.040	0.029	0.029
$\langle u_z^2u_x^2\rangle$	0.043	0.043	0.014	0.014
$\langle u_x^5\rangle$			−0.0007	
$\langle u_y^4u_x\rangle$			0.0046	
$\langle u_z^4u_x\rangle$			0.0003	
$\langle u_x^3u_y^2\rangle$			0.0009	
$\langle u_x^3u_z^2\rangle$			0.0001	
$\langle u_y^2u_z^2u_x\rangle$			0.0005	
$\langle u_x^6\rangle$	0.0062		0.0008	
$\langle u_y^6\rangle$	0.0043		0.0085	
$\langle u_z^6\rangle$	0.0040		0.0009	
$\langle u_x^4u_y^2\rangle$	0.0010		0.0003	
$\langle u_x^4u_z^2\rangle$	0.0010		0.0002	
$\langle u_y^4u_z^2\rangle$	0.0009		0.0008	
$\langle u_y^4u_z^2\rangle$	0.0009		0.0007	
$\langle u_z^4u_x^2\rangle$	0.0009		0.0002	
$\langle u_z^4u_y^2\rangle$	0.0009		0.0004	
$\langle u_x^2u_y^2u_z^2\rangle$	0.0001		0.0001	

Table 2. *The determined OPP parameters*

The results analysed by the OPP model up to second, third and fourth order are listed in each column.

Units are eV Å^{-n}.

	Ti atom		O atom		
	Second	Fourth	Second	Third	Fourth
α_{11}	1.956 (1)	2.1399 (3)	3.983 (5)	3.914 (2)	3.890 (2)
α_{22}	2.143 (1)	2.3386 (4)	1.889 (2)	1.8149 (9)	1.855 (1)
α_{33}	2.136 (1)	2.3243 (4)	3.436 (5)	3.422 (2)	3.557 (2)
β_{111}				3.67 (1)	3.37 (1)
β_{221}				−5.84 (1)	−5.68 (1)
β_{331}				−2.34 (3)	−2.25 (2)
γ_{1111}		−3.583 (3)			−2.09 (5)
γ_{2222}		−3.477 (6)			−1.46 (1)
γ_{3333}		−3.187 (7)			−5.77 (8)
γ_{1122}		−4.47 (2)			7.2 (1)
γ_{2233}		−8.53 (2)			−1.5 (1)
γ_{3311}		−4.75 (2)			0.7 (3)
$R(\rho)$ (%)	3.98	0.73	8.83	4.34	3.83
$wR(\rho)$ (%)	6.43	1.31	15.74	5.94	5.08

refinement are given as

$$R(\rho) = \sum_{u^2 \le R_0^2} |\rho'_{\mathrm{MEM}}(\mathbf{u}) - \rho_{\mathrm{OPP}}(\mathbf{u})| \Big/ \sum_{u^2 \le R_0^2} |\rho'_{\mathrm{MEM}}(\mathbf{u})| \tag{13}$$

and

$$wR(\rho) = \left\{ \sum_{u^2 \le R_0^2} \omega(\mathbf{u}) [\rho'_{\mathrm{MEM}}(\mathbf{u}) - \rho_{\mathrm{OPP}}(\mathbf{u})]^2 \times \left[\sum_{u^2 \le R_0^2} \omega(\mathbf{u}) \rho'^2_{\mathrm{MEM}}(\mathbf{u}) \right]^{-1} \right\}^{1/2}, \tag{14}$$

where $wR(\rho)$ is a weighted reliability factor and a newly added criterion. Since the OPP model is based on the Einstein oscillator theory, the least-squares refinement is carried out on each atom. The potential parameters obtained for each atom are listed in Table 2. For the Ti atom, nine OPP parameters, of which three are harmonic and six are fourth-order anharmonic, are determined with $R = 0.73$ and $wR = 1.31\%$. For the O atom, twelve OPP parameters, of which three are harmonic, three are third- and six are fourth-order anharmonic, are determined with $R = 3.83$ and $wR = 5.08\%$. The results analysed by the OPP model up to second- and third-order terms are also listed in Table 2 for comparison. It is found that the fitting becomes better as the effective order of the OPP is increased for both Ti and O atoms. In particular, the drastic improvements between the second- and third-order analysis for the O atom and between the second- and fourth-order analysis for the Ti atom are recognized. These results show that anharmonic terms are needed to represent the precise thermal vibration of rutile. It is also understood in Table 2 that lower-order parameters are almost unchanged when higher-order terms are added in the OPP. This means that the correlation between the anharmonic terms is sufficiently small. Consequently, the anharmonic terms can be regarded as small perturbations.

The TSF map calculated from (5) is shown in Fig. 6 for (110) and (002) planes. Each map is calculated by the OPP model up to second, third and fourth orders. Comparison of these maps with the MEM density maps shown in Fig. 2 indicates that the TSF maps up to fourth-order parameters show the best fitting with the MEM density maps. For the O atom, the density distribution changed drastically between the second- and third-order analyses, as is expected from the reliability factors. The skewness of the O atom is very well reconstructed by the third-order anharmonicities. For the Ti atom, there is slight anisotropy on the *XY* and *XZ* planes in the MEM maps. This anisotropy is well constructed by the fourth-order analysis. It can be said that the anisotropy of the Ti atom is mainly due to the fourth-order anharmonicities.

In step 4, the OPP higher-order moments are calculated from (9) by using the obtained parameters of the fourth-order analysis. The results are listed in Table 1 together with the MEM higher-order moments. It is judged from the table that the agreements are satisfied over all the orders. Then no further analysis is carried out. It is worthwhile to compare the obtained OPP second-order moments with the previous results of Rietveld analysis (Howard, Sabine & Dickson, 1991), which are listed in Table 3. For the O atom, both the second-order moment of the OPP and the thermal parameter of the Rietveld analysis are almost equal within the standard deviations of the Rietveld analysis. For the Ti atoms, the discrepancy is larger than in the O-atom case. This might be due to the correlation between the harmonic and the fourth-order anharmonic terms because the Ti-atom analysis has slightly bigger correlation-matrix elements than the O-atom analysis.

5. The reliability against the observed structure factors

In the least-squares analysis, the estimated standard deviation (e.s.d.) of each parameter is defined as inversely proportional to the difference between the number of data and number of parameters. In the present analysis, the number of data that satisfy $\mathbf{u}^2 \le R_0^2$ is 30 399 pixels and the number of parameters is at most 12. This causes the unrealistic small e.s.d.'s. This is because the potential parameters are not refined directly with the experimentally observed values. At this stage, a realistic measure of e.s.d. against the observed data has not been performed. In order to examine how accurately the potential parameters are determined with respect to the experimental observables, the following reliability factors are calculated.

$$R(\mathrm{SF}) = \left[\sum |F_{\mathrm{OBS}}(\mathbf{h}) - F_{\mathrm{OPP}}(\mathbf{h})| + \sum |G_{\mathrm{OBS}}(i) - G_{\mathrm{OPP}}(i)| \right] \times \left[\sum |F_{\mathrm{OBS}}(\mathbf{h})| + \sum |G_{\mathrm{OBS}}(i)| \right]^{-1} \tag{15}$$

and

$$wR(\mathrm{SF}) = \left(\{\sum[F_{\mathrm{OBS}}(\mathbf{h}) - F_{\mathrm{OPP}}(\mathbf{h})]^2/\sigma(\mathbf{h})^2 + \sum[G_{\mathrm{OBS}}(i) - G_{\mathrm{OPP}}(i)]^2/\sigma(i)^2\} \times \left[\sum F_{\mathrm{OBS}}(\mathbf{h})^2/\sigma(\mathbf{h})^2 + \sum G_{\mathrm{OBS}}(i)^2/\sigma(i)^2\right]^{-1}\right)^{1/2}, \quad (16)$$

where $F_{\mathrm{OBS}}(\mathbf{h})$ and $G_{\mathrm{OBS}}(i)$ are the observed structure factors of individual and overlapped reflections, $\sigma(\mathbf{h})$ and $\sigma(i)$ are their standard deviations and $F_{\mathrm{OPP}}(\mathbf{h})$ is calculated from

$$F_{\mathrm{OPP}}(\mathbf{h}) = \sum_{r_c} \sum_{u^2 \le R_0^2} \rho_{\mathrm{OPP}}(\mathbf{u}) \exp[2\pi i \mathbf{h}(\mathbf{r}_c + Q^{-1}\mathbf{u})]. \quad (17)$$

The structure factor for the overlapped reflections, $G(i)$, is introduced to give a combined structure factor for the overlapped peaks for the powder diffraction experiment (Sakata, Mori, Kumazawa, Takata & Toraya, 1990). These reliability factors are expressed as the agreement between the experimentally observed data, $F_{\mathrm{OBS}}(\mathbf{h})$ and $G_{\mathrm{OBS}}(i)$, and the structure factors, $F_{\mathrm{OPP}}(\mathbf{h})$ and $G_{\mathrm{OPP}}(i)$, calculated from the refined potential parameters.

Table 3. *The second-order moments calculated by the thermal vibration parameters U_{11}, U_{22}, U_{12} and U_{33} of the Rietveld analysis (Howard, Sabine & Dickson, 1991)*

Units are Å^2 × 10^{-3}.

	Ti atom	O atom
$\langle u_x^2 \rangle = U_{11} + U_{12}$	6.4 (4)	3.2 (2)
$\langle u_y^2 \rangle = U_{11} - U_{12}$	7.2 (4)	7.2 (2)
$\langle u_z^2 \rangle = U_{33}$	4.6 (5)	3.5 (2)

The results are listed in Table 4. When the OPP model is effective in the refinement, the reliability factors become smaller. This tendency is quite similar to the case of the reliability factors of the least-squares refinement calculated by (13) and (14) in real space. Therefore, it is confirmed that the fourth-order analysis also shows the best-fitting result among the present anharmonic analyses with respect to the observed structure factors. The reliability factors against the $F_{\mathrm{MEM}}(\mathbf{h})$, which is

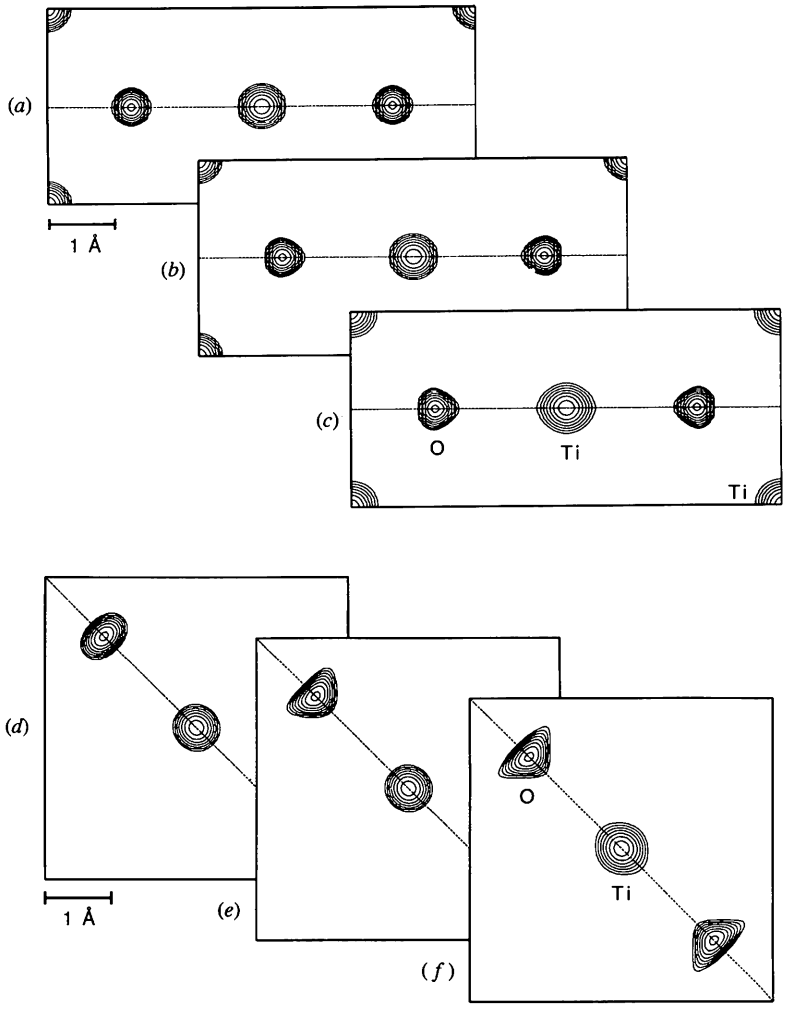

Fig. 6. The TSF maps calculated by the obtained OPP model. (*a*), (*b*) and (*c*) are (110) planes and (*d*), (*e*) and (*f*) are (002) planes. (*a*) and (*d*) are calculated by the OPP function up to second-order parameters for both atoms, (*b*) and (*e*) up to second order for the Ti atom and third order for the O atom, (*c*) and (*f*) up to fourth order for both atoms. The contour lines are the same as in Fig. 2.

Table 4. *List of structure factors and reliability factors with respect to the observed structure factors, F_{OBS}*

The F_{MEM} column shows the results of the MEM analysis. The F_{OPP} columns labelled [2], [3] and [4] are the values calculated by the second-, third- and fourth-order analyses.

h	k	l	F_{OBS}	F_{MEM}	F_{OPP}[2]	F_{OPP}[3]	F_{OPP}[4]
1	1	0	−4.34	−4.18	−4.21	−4.14	−4.17
1	0	1	−14.56	−14.40	−14.17	−14.37	−14.40
2	0	0	−24.21	−24.22	−23.79	−24.10	−24.14
1	1	1	−20.16	−20.18	−19.71	−20.09	−20.11
2	1	0	13.60	13.59	13.26	13.58	13.59
2	2	0	6.55	6.68	6.46	6.60	6.59
0	0	2	15.77	16.01	15.48	15.95	15.95
3	1	0	−12.67	−12.69	−12.53	−12.69	−12.71
2	2	1	−8.66	−8.72	−8.52	−8.74	−8.75
3	0	1	12.62	12.52	12.13	12.52	12.52
1	1	2	−4.04	−3.91	−3.94	−3.89	−3.90
3	1	1	10.47	10.52	10.32	10.41	10.42
3	2	0	−7.56	−7.40	−7.21	−7.35	−7.35
2	0	2	−23.30	−23.29	−22.88	−23.17	−23.21
2	1	2	13.12	13.13	12.82	13.12	13.14
3	2	1	−20.59	−20.66	−20.35	−20.60	−20.63
4	1	0	−19.63	−19.69	−19.32	−19.64	−19.65
2	2	2	6.43	6.59	6.37	6.51	6.50
3	3	0	9.32	9.35	9.06	9.40	9.40
4	1	1	−7.78	−7.75	−7.67	−7.70	−7.72
3	1	2	12.22	−12.14	−11.99	−12.14	−12.17
4	2	0	−8.88	−8.81	−8.80	−8.69	−8.70
3	3	1	−5.08	−4.98	−4.98	−4.89	−4.89
4	2	1	12.93	12.94	12.68	12.95	12.96
1	1	3	−18.82	−18.87	−18.43	−18.79	−18.80
4	3	0	10.47	10.48	10.34	10.39	10.40
3	3	2	9.36	9.15	8.88	9.20	9.20
5	1	1	2.45	2.89	2.87	3.02	3.03
3	0	3	11.66	11.93	11.58	11.94	11.93
5	2	1	9.46	9.47	9.31	9.39	9.39
3	1	3	10.05	9.85	9.65	9.74	9.75
4	4	0	−6.53	−6.03	−5.87	−6.06	−6.07
5	3	0	−22.34	−22.34	−22.04	−22.20	−22.33
4	4	1	−19.05	−18.84	−18.55	−18.82	−18.84
6	1	0	16.11	16.01	15.79	15.87	15.88
h	k	l	G_{OBS}	G_{MEM}	G_{OPP}[2]	G_{OPP}[3]	G_{OPP}[4]
3	2	2	9.74	9.60	9.42	9.57	9.59
1	0	3					
4	1	2	13.50	13.46	13.22	13.43	13.44
2	1	3					
4	3	1	14.98	15.03	14.84	14.98	15.00
5	0	1					
4	2	2	8.47	8.27	8.18	8.23	8.24
2	2	3					
4	3	2	15.48	15.28	15.06	15.22	15.24
3	2	3					
R(SF) (%)				0.91	2.25	1.12	1.06
wR(SF) (%)				0.76	2.12	0.94	0.88

calculated from ρ_{MEM}, are also listed in Table 4. Since the potential-parameter analysis is performed with ρ_{MEM}, the reliability factors of the fourth-order analysis show the best agreement with those of $F_{MEM}(\mathbf{h})$.

6. Concluding remarks

The OPP parameters of rutile are accurately determined by the least-squares refinement of the MEM nuclear density distribution. The obtained OPP model is represented by up to fourth-order terms and the TSF shows excellent agreement with the MEM nuclear density distribution. Moreover, the fourth-order analysis also shows the best fit with respect to the observed structure factors. The present work is a good demonstration that the potential parameters can be precisely determined even in a powder diffraction case. This work reveals the possibility of a new thermal-vibration analysis in crystallography.

The authors thank Dr C. J. Howard for providing his neutron powder diffraction data. The authors also thank Professors J. Harada and K. Ishida for their encouragement. Most of the computations were performed at the Computation Centers of Nagoya University and Science University of Tokyo, which are gratefully acknowledged by the authors. This work has been partly supported by a Grant in Aid of Scientific Research from the Ministry of Education, Science and Culture of Japan.

References

HOWARD, C. J., SABINE, T. M. & DICKSON, F. (1991). *Acta Cryst.* B**47**, 462–468.

KUBOTA, Y., TAKATA, M. & SAKATA, M. (1993). *J. Phys. Condens. Matter*, **5**, 8245–8254.

KUMAZAWA, S., KUBOTA, Y., TAKATA, M., SAKATA, M. & ISHIBASHI, Y. (1993). *J. Appl. Cryst.* **26**, 453–457.

SAKATA, M., MORI, R., KUMAZAWA, S., TAKATA, M. & TORAYA, H. (1990). *J. Appl. Cryst.* **23**, 526–534.

SAKATA, M. & SATO, M. (1990). *Acta Cryst.* A**46**, 263–270.

SAKATA, M., UNO, T., TAKATA, M. & HOWARD, C. J. (1993). *J. Appl. Cryst.* **26**, 159–164.

SAKATA, M., UNO, T., TAKATA, M. & MORI, R. (1992). *Acta Cryst.* B**48**, 591–598.

SAKATA, M., UNO, T., TAKATA, M., TAKAGI, M., KUMAZAWA, S. & HOWARD, C. J. (1994). Proc. of the 5th International Symposium on Advanced Nuclear Energy Research.

SAKURAI, T. (1972). *X-ray Crystal Analysis*. Tokyo: Syokaho. (In Japanese.)

TAKATA, M., SAKATA, M., KUMAZAWA, S., LARSEN, F. K. & IVERSEN, B. B. (1994). *Acta Cryst.* A**50**, 330–337.

TANAKA, K. & MARUMO, F. (1983). *Acta Cryst.* A**39**, 631–641.

WILLIS, B. T. (1969). *Acta Cryst.* A**25**, 277–300.